# Reconstruction of Corrupted Photoplethysmography Signals to Facilitate Continuous Monitoring

Aikaterini Vraka[1], Juan M. Gracia-Baena[2], Flavia Ravelli[3], Philip Langley[4], Raúl Alcaraz[5], José J Rieta[1]

[1] BioMIT.org, Electronic Engineering Department, Universitat Politecnica de Valencia, Spain
[2] Cardiovascular Surgery Department, Hospital Clínico Universitario de Valencia, Spain
[3] Department of Cellular, Computational and Integrative Biology (CIBIO), University of Trento, Italy
[4] Department of Engineering, University of Hull, United Kingdom
[5]Research Group in Electronic, Biomed. and Telecomm. Eng., Univ. of Castilla-La Mancha, Spain

## Abstract

*Photoplethysmography (PPG) is the leading technology behind wearables, significantly hindered by PPG's susceptibility to motion artifacts (MAs). This study presents a PPG reconstruction algorithm operating regardless of the source of noise. Artifact detection is initially performed by spectral and amplitude-based control. Morphology, spectral and heart-rate (HR) variability (HRV) information of the adjacent clean segments are used for reconstruction. Thirty-six originally clean PPGs with added noise of 2–120 s were used. Recordings were resampled to 250 Hz. HR and HRV features were compared between original and reconstructed PPGs via Pearson correlation ($\rho$), Bland-Altman (BA), normalized root mean square error (nRMSE) and mean absolute percentage error (MAPE) analysis. For HR, $\rho > 0.9$ for all noise lengths. Time-domain HRV: $\rho > 0.91$. Frequency-domain HRV: $\rho > 0.75$. Poincaré indices: $\rho > 0.85$. Max. nRMSE: $0.58\%$, max. MAPE: $1.72\%$. At least $86\%$ of recordings were within confidence interval, with most results being between $89\%-97\%$, regardless of the noise duration. The proposed algorithm allows the reconstruction of corrupted PPG signals. The noise duration cut-off for optimal results is 30–45 s. Nevertheless, it can be applied in longer segments, still providing satisfactory results.*

## 1. Introduction

Photoplethysmography (PPG) is gaining increasing attention due to its simple technology and versatility regarding use scenarios [1, 2]. Among the diverse applications, PPG has been proved especially useful in healthcare, allowing remote health monitoring and hence, prevention of diseases [1, 2]. PPG signal can be analyzed either in its primal form or after further processing, with the most popular applications being blood pressure or heart-rate (HR) variability (HRV) calculation [3, 4]. The main limitation of PPG, however, is the extreme sensitivity to any source of noise, with motion artifacts (MAs) being the dominant issue [1, 3]. Noise significantly affects PPG signal quality and complicates the continuous health tracking.

Many works have focused on MAs detection [5–7]. The principal techniques used are signal decomposition, adaptive filtering and spectral/morphological analysis [5]. Signal decomposition methods operate by locating MAs with the help of other signal sources and decide upon the usability of the signal based on quality analysis [5]. Adaptive filters also make use of other sources to detect and remove the noisy components of the signals [5]. Nevertheless, typical references used in adaptive filtering are not considered reliable in detecting noise due to minimal movement [6]. The final and most diverse MA detection category often requires the use of additional signal sources as well, while in some cases, it is significantly hindered by the overlapping of noise and HR dominant frequencies (DF) [5, 7].

Besides the usual requirement of additional signal sources, which are not always available, the main drawback of the aforementioned techniques is the hyperfocus on MA detection: noise is indeed detected but the signal is discarded or partially used in the best case scenario. Moreover, while most of the algorithms are MA-centered, the truth is that other sources of noise as well might affect PPG quality and make its analysis impossible, obstructing continuous health monitoring. The current work presents a simplified technique to take full advantage of the corrupted signals that can operate with any type of noise.

## 2. Materials and Methods

The database consisted of 36 PPG signals from 17 critically-ill patients, utilizing the BIDMC PPG and Respi-

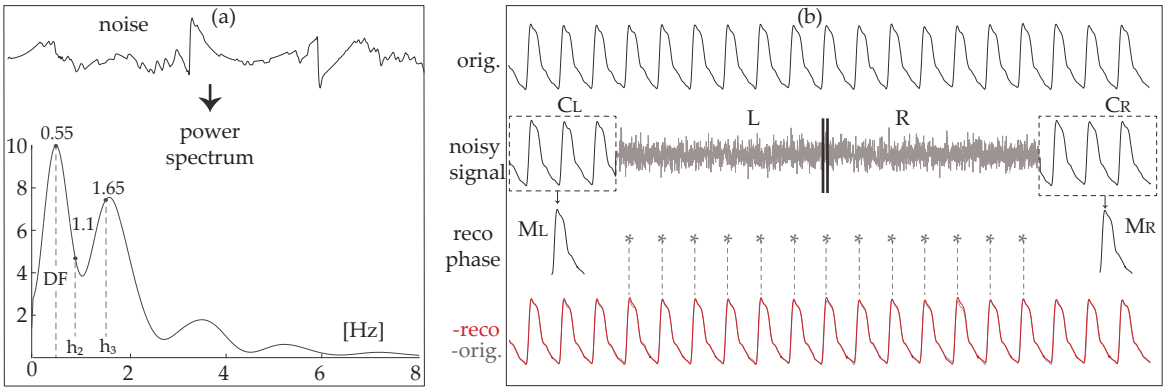


Figure 1. (a) Detection of noise due to lack of peak in the 0.7-Hz window of the second harmonic (0.75-1.45 Hz); (b) An example of PPG reconstruction. Noise is added to the original signal and the reconstruction starts by defining $C_{L,R}$ and splitting noise in L, R. The pulse morphology ($M_{L,R}$) at each segment is then defined from $C_{L,R}$ and the pulse peak locations are also defined (*). The reconstructed (red) and original (gray) signals are shown in the bottom. The gray signal is hardly visible as it converges with the reconstructed signal.

ration Dataset [8]. Each signal had an eight-minute duration and was extracted with 125 Hz sampling frequency. In order to ensure that the signal resolution was appropriate for the analysis, signals were resampled to 250 Hz.

Preprocessing started by a 2nd-order high-pass Butterworth filter with cut-off frequency at $0.5$ Hz, followed by a 3-level discrete wavelet transform to remove baseline fluctuation and high frequency noise, respectively. Then, random noise was added to the originally clean signals. For each clean signal, 11 corrupted signals were created with a noise duration of $2, 5, 10, 20, 30, 45, 60, 75, 90, 105$ and $120$ s. The mean signal-to-noise ratio of corrupted segments was $-21.67$ dB.

The main analysis was separated into two phases, the noise detection and the PPG reconstruction phases, each performed by making exclusive use of PPG signals.

## A. Noise detection phase

The first step of noise detection was segmentation into 8-s epochs with 75% overlapping, meaning that the minimum noise length that can be detected is of 2 s. An exhaustive noise detection process was performed in three levels, starting by localizing the epochs with DF that do not belong to the $[0.3 - 4]$ Hz interval. Afterwards, the sum of the spectral power at 0.7-Hz windows with DF and the first two harmonics centered ($SP_{DF,2,3}$) was calculated and compared to the total spectral power of the epoch ($SP_{all}$), so that a segment was considered as noisy if $SP_{DF,2,3} < 0.65 \times SP_{all}$. The final noise detection level consisted of the detection of all those segments for which a peak in each 0.7-Hz window could not be found. An example of noise detected due to lack of spectral peaks is illustrated in Figure 1.a. When the noise detection process was over, the noise tagging was extended by 1 s left and right of the noisy segment, in order to include cases of undetected noise segment in transition.

## B. PPG reconstruction phase

In order to reconstruct the noisy PPG, the nearest clean segments at the left and right of the noise ($C_{L,R}$) need to be located and used as reference. Their DF is then calculated by a second derivative analysis [9]. The noisy segment was separated into two equal parts (L, R) and the $DF_{L,R}$ and $HR_{L,R}$ of each part was calculated, following a 2nd-order band-pass Butterworth filter with $f_{c1,c2} = DF_{C_L,C_R} \pm 0.35$. Afterwards, HRV and amplitude variability of $C_{L,R}$ were calculated by using the 10 closest peaks of each segment ($HRV_{L,R}$ and $A_{L,R}$, respectively). The baseline pulse morphology of L and R ($M_{L,R}$) was also defined by the median of the five closest pulses of $C_{L,R}$. Reconstruction started by defining the peak locations of the reconstructed segments, by considering the $HR_{L,R}$ and $HRV_{L,R}$. Pulse recreation was effectuated by using $M_{L,R}$ with its length and amplitude modified so that it converges with the reconstructed peak locations, while considering the $A_{L,R}$. An example of PPG reconstruction can be seen in Figure 1.b.

In order to evaluate the ability of the method to faithfully resemble the non-corrupted signal, the original and corrupted signals were compared. HR and HRV (SDNN, VARNN, RMSSD, VLF, LF, HF, SD1, SD2 [10]) were calculated in both signals. Comparison was performed via Pearson correlation and Bland-Altman (BA) analysis [11]. Finally, normalized RMS error (nRMSE) and mean absolute percentage error (MAPE) were calculated, using the HRV of the clean PPG signals as reference [12, 13].

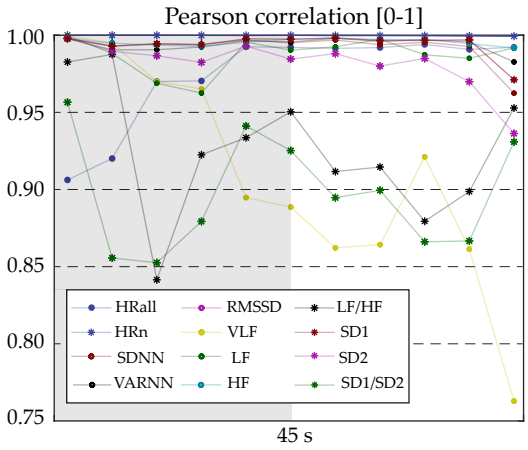


Figure 2. Pearson correlation for HR and HRV. Correlation is quite high for most features until 45 s. RMSSD and SD1 correlations converge for all noise lengths.

## 3. Results

Figure 2 illustrates the Pearson correlation between original and reconstructed PPGs for HR and all HRV features. HR correlation was performed both in the entire signal ($HR_{all}$) and exclusively in the noisy segment ($HR_n$). Overall, correlations were high in most cases, with even the lowest correlation in 120 s noise being higher than $75\%$, while values being mostly higher than 90% or 95%. More specifically, HR and time-domain HRV features showed an almost perfect correlation with values higher than $95\%$ regardless of the noise length. While an almost perfect correlation was also found for HF, the remaining frequency-domain features showed correlations as low as $76\%$. Nevertheless, correlations were close to or higher than $85\%$ in all cases with noise lower than 120 s. Regarding Poincare indices, while SD1 and SD2 showed very high correlations, correlation in SD1/SD2 was lower but still acceptable, being $\geq 85\%$.

The results of BA analysis are then shown in Table 1, where the percentage $(0-1)$ of recordings within the confidence interval (CI) can be seen. This percentage oscillates between $86-97\%$, with $86\%$ being seen only twice, while being $93\%$ or more in most cases. These results indicate coherence between HR and HRV values of the original and the reconstucted PPG signals. In the last two rows of the same table, the results of the error analysis can be seen. Error was maintained very low regardless of the error metric and the noise length, showing values $< 2\%$. nRMSE stayed below $0.6\%$ for all cases, while MAPE showed values $< 1\%$ for noise length up to 30 s. Regardless of the error metric, it seems that the error increases proportionately to the duration of the noise.

## 4. Discussion

MA detection and elimination in PPG recordings is a puzzling yet necessary task [1, 3]. Unfortunately, most works only focus on the first part, developing complex algorithms often requiring additional signals in order to detect MAs [5–7]. This strategy has significant limitations: additional signal sources might not be available, while MAs is the main but not the only source of noise. The most significant drawback, however, is the fact that, although the noise is indeed detected, the signal is in most cases discarded, which makes the initial effort put to find the noise pointless.

This study presented a simple and efficient algorithm that not only detects noise using exclusively PPG signals

Table 1. Results of BA (CI) and error analysis for different noise lengths. $90\%$ or more of the recordings are within CI in most cases. MAPE stays below $1.00$ for noise $\leq 30$ s. nRMSE is below $1.00$ regardless of the noise duration.

| | 2 s | 5 s | 10 s | 20 s | 30 s | 45 s | 60 s | 75 s | 90 s | 105 s | 120 s | |
|---|---|---|---|---|---|---|---|---|---|---|---|---|
| $HR_n$ | 0.97 | 0.86 | 0.97 | 0.93 | 0.97 | 0.97 | 0.93 | 0.97 | 0.97 | 0.97 | 0.97 | |
| $HR_all$ | 0.93 | 0.93 | 0.93 | 0.93 | 0.97 | 0.89 | 0.97 | 0.93 | 0.93 | 0.93 | 1.00 | |
| SDNN | 0.97 | 0.89 | 0.93 | 0.93 | 0.93 | 0.89 | 0.93 | 0.89 | 0.89 | 0.97 | 0.93 | |
| VARNN | 0.97 | 0.89 | 0.93 | 0.89 | 0.89 | 0.86 | 0.93 | 0.93 | 0.89 | 0.93 | 0.97 | |
| RMSSD | 0.97 | 0.97 | 0.97 | 0.93 | 0.93 | 0.93 | 0.93 | 0.89 | 0.89 | 0.93 | 0.97 | |
| VLF | 0.93 | 0.97 | 0.97 | 0.97 | 0.93 | 0.97 | 0.93 | 0.93 | 0.93 | 0.93 | 0.93 | **BA:CI** |
| LF | 0.93 | 0.93 | 0.93 | 0.97 | 0.93 | 0.93 | 0.93 | 0.97 | 0.89 | 0.93 | 0.97 | |
| HF | 0.89 | 0.93 | 0.93 | 0.93 | 0.93 | 0.93 | 0.93 | 0.89 | 0.89 | 0.89 | 0.97 | |
| LF/HF | 0.93 | 0.89 | 0.93 | 0.93 | 0.93 | 0.93 | 0.97 | 0.93 | 0.97 | 0.97 | 0.97 | |
| SD1 | 0.97 | 0.97 | 0.97 | 0.93 | 0.93 | 0.93 | 0.93 | 0.89 | 0.89 | 0.93 | 0.97 | |
| SD2 | 0.93 | 0.93 | 0.93 | 0.97 | 0.97 | 0.97 | 0.89 | 0.93 | 0.93 | 0.89 | 0.93 | |
| SD1/SD2 | 0.97 | 0.89 | 0.93 | 0.93 | 0.97 | 0.97 | 0.89 | 0.97 | 0.97 | 0.97 | 0.97 | |
| nRMSE [%] | 0.07 | 0.08 | 0.09 | 0.15 | 0.20 | 0.32 | 0.27 | 0.35 | 0.38 | 0.47 | 0.58 | **Error** |
| MAPE [%] | 0.59 | 0.60 | 0.67 | 0.81 | 0.96 | 1.22 | 1.24 | 1.24 | 1.14 | 1.51 | 1.72 | |

but is also able to retrieve the information even in the case that the signal quality is very low. The noise detection phase consists of a three-round control, based on the DF of the signal. The PPG reconstruction phase is based on a simple assumption: in very short segments of 1-2 s, even when the activity of the subject is abruptly modified, there will be high similarity in the morphology and the DF of the PPG signal. Starting from this point, the algorithm uses the clean segments surrounding the noise in order to iteratively reconstruct the signal. As a result, there is high resemblance between the original and the reconstructed signals, as can be seen from Figure 1.

Given that HRV is more sensitive to even the slightest alterations in HR, the performance was tested in terms of correlation, BA and error analysis. Pearson correlations asseses the similarity between the patterns of the original and the reconstructed signals and was overall found high, especially in time-domain HRV analysis. A more adequate assessment of the similarities between two signals can be performed with BA analysis, using the original PPG signals as the reference. Indeed, the results indicated a general agreement, an observation that was corroborated by the very low error rates even in the cases of the longest noise. These results suggest the use of the proposed algorithm in health monitoring analyses or its implementation in continuous monitoring devices, significantly contributing to the uninterrupted health tracing.

## 5. Conclusions

A simple algorithm was presented able to detect noise of any source and efficiently retrieve the lost information of the signal. The algorithm was evidenced successful in faithfully recreating the distorted signal and calculating crucial indices in healthcare analysis such as HRV features. The use of this technique in wearable devices could assist in health analysis and thereby contribute to prevention from cardiovascular diseases.

## Acknowledgments

Funding grants PID2021-00X128525-IV0 and PID2021-123804OB-I00 from Spanish Government and European Regional Development Fund (10.13039/501100011033), SBPLY/17/180501/000411 from Junta de Castilla-La Mancha and AICO/2021/286 from Generalitat Valenciana.

## References

[1] Allen J. Photoplethysmography and its application in clinical physiological measurement. Physiological measurement March 2007;28:R1–39. ISSN 0967-3334.

[2] Labati RD, Piuri V, Rundo F, Scotti F. Photoplethysmographic biometrics: A comprehensive survey. Pattern Recognition Letters 2022;.

[3] Castaneda D, Esparza A, Ghamari M, Soltanpur C, Nazeran H. A review on wearable photoplethysmography sensors and their potential future applications in health care. International journal of biosensors bioelectronics 2018;4:195–202. ISSN 2573-2838.

[4] Maity AK, Veeraraghavan A, Sabharwal A. Ppgmotion: Model-based detection of motion artifacts in photoplethysmography signals. Biomedical Signal Processing and Control 2022;75:103632.

[5] Polak AG, Klich B, Saganowski S, Prucnal MA, Kazienko P. Processing photoplethysmograms recorded by smartwatches to improve the quality of derived pulse rate variability. Sensors Basel Switzerland September 2022;22. ISSN 1424-8220.

[6] Lee H, Chung H, Ko H, Parisi A, Busacca A, Faes L, Pernice R, Lee J. Adaptive scheduling of acceleration and gyroscope for motion artifact cancelation in photoplethysmography. Computer methods and programs in biomedicine September 2022;226:107126. ISSN 1872-7565.

[7] Moscato S, Giudice SL, Massaro G, Chiari L. Wrist photoplethysmography signal quality assessment for reliable heart rate estimate and morphological analysis. Sensors Basel Switzerland August 2022;22. ISSN 1424-8220.

[8] Pimentel MA, Johnson AE, Charlton PH, Birrenkott D, et al. Toward a robust estimation of respiratory rate from pulse oximeters. IEEE Transactions on Biomedical Engineering 2016;64(8):1914–1923.

[9] Anisimov A, Alekseev B, Egorov D. Comparison of heart rate derived from ecg and pulse wave signals during controlled breathing test for biofeedback systems. In 2021 IEEE Ural-Siberian Conference on Computational Technologies in Cognitive Science, Genomics and Biomedicine (CSGB). 2021; 430–434.

[10] Heart rate variability. standards of measurement, physiological interpretation, and clinical use. task force of the european society of cardiology and the north american society of pacing and electrophysiology. European heart journal March 1996;17:354–381. ISSN 0195-668X.

[11] Altman DG, Bland JM. Measurement in medicine: The analysis of method comparison studies. Journal of the Royal Statistical Society Series D The Statistician 1983; 32:307. ISSN 0039-0526.

[12] Armstrong J, Collopy F. Error measures for generalizing about forecasting methods: Empirical comparisons. International Journal of Forecasting 1992;8(1):69–80. ISSN 0169-2070.

[13] Swamidass PM (ed.). MAPE (mean absolute percentage error). Boston, MA: Springer US. ISBN 978-1-4020-0612-8, 2000; 462–462.

Address for correspondence:

José J. Rieta

BioMIT.org, Electronic Engineering Department, Building 7F, Universitat Politecnica de Valencia, 46022 Valencia, Spain.

e-mail: jjrieta@upv.es